FULL PAPER

ADVANCED
HEALTHCARE
MATERIALS

www.advhealthmat.d

Check for updates

Exploring Circulating Tumor Cells in Cholangiocarcinoma Using a Novel Glycosaminoglycan Probe on a Microfluidic Platform

Priya Gopinathan, Nai-Jung Chiang, Anandaraju Bandaru, Anirban Sinha, Wen-Yen Huang, Shang-Cheng Hung,* Yan-Shen Shan,* and Gwo-Bin Lee*

The search of alternative approaches to epithelial cell adhesion molecule (EpCAM), for the isolation of circulating tumor cells (CTC), is on the rise. This work attempts at evaluating the feasibility of using a new glycosaminoglycan, SCH45, as a probe to isolate CTCs from the peripheral blood of 65 advanced/metastatic cholangiocarcinoma (CCA) patients. The positive enrichment of CTCs from 1 mL of blood using SCH45-bound magnetic beads and subsequent staining on an integrated microfluidic platform is demonstrated. Results detailing CTC concentrations averaging ≥1 CTCs mL^{-1} of blood are shown, and a conventional protein biomarker, EpCAM, has been used to corroborate the finding that 100% of the patients possess CTCs in their blood. Studies detailing the use of CTCs in the prognostic monitoring and treatment effectiveness of advanced/metastatic CCA are scarce, and the isolation of CTCs from all CCA patients tested has not been reported yet. A strong correlation between CTC counts and disease progression at the time of and/or in advance of radiographic imaging in patients receiving chemotherapy is also reported. This study is one of its kind with the new probe and reduced sample volume and has potential for use in CCA diagnosis and prognosis in the near future.

1. Introduction

Among liver cancers, cholangiocarcinoma (CCA) is the second most common primary hepatobiliary malignancy and is typically characterized by late-stage diagnosis, poor prognosis, high recurrence, and frequent metastasis.[1] CCA is an aggressive malignancy of epithelial origin, with markers of cholangiocyte differentiation, and its overall incidence has increased dramatically in the past decades.[2] The disease presents itself in advanced stages, at which point surgical resection and curative liver transplantation remain the mainstays of potentially curative treatment. Unfortunately, early diagnosis of CCA poses a challenge owing to its "silent" clinical characteristics. Further challenging is the diagnosis owing to difficulty in tumor sample collection for pathological confirmation.[3]

Advancements in molecular technologies have led to the discovery of many new

Dr. P. Gopinathan, Dr. A. Sinha, Prof. G.-B. Lee
Institute of Nanoengineering and Microsystems
National Tsing Hua University
Hsinchu 30013, Taiwan
E-mail: gwobin@pme.nthu.edu.tw

Dr. N.-J. Chiang, Prof. Y.-S. Shan
Institute of Clinical Medicine
College of Medicine
National Cheng Kung University
Tainan 70457, Taiwan
E-mail: sshan@mail.ncku.edu.tw

Dr. N.-J. Chiang
National Institute of Cancer Research
National Health Research Institutes
Miaoli 35053, Taiwan

Dr. N.-J. Chiang
Department of Internal Medicine
National Cheng Kung University Hospital
College of Medicine
National Cheng Kung University
Tainan 70403, Taiwan

Dr. A. Bandaru, Prof. S.-C. Hung
Genomics Research Centre
Academia Sinica
Taipei, Taiwan 11529, Republic of China
E-mail: schung@gate.sinica.edu.tw

Dr. W.-Y. Huang, Prof. G. B. Lee
Department of Power Mechanical Engineering
National Tsing Hua University
Hsinchu City 30013, Taiwan

Prof. S.-C. Hung
Department of Applied Science
National Taitung University
Taitung 95053, Taiwan

Prof. Y.-S. Shan
Department of Surgery
National Cheng Kung University Hospital
College of Medicine
National Cheng Kung University
Tainan 70403, Taiwan

Prof. G. B. Lee
Institute of Biomedical Engineering
National Tsing Hua University
Hsinchu 30013, Taiwan

The ORCID identification number(s) for the author(s) of this article can be found under https://doi.org/10.1002/adhm.201901875.

ADVANCED
SCIENCE NEWS
www.advancedsciencenews.com

ADVANCED
HEALTHCARE
MATERIALS
www.advhealthmat.de

cancer biomarkers that have been shown to have utility in the 1) prediction of treatment response and 2) post-treatment monitoring of various types of cancers.[4] Circulating tumor cells (CTCs) were first identified more than a century ago (while posthumously investigating the blood of a highly metastatic breast cancer patient[5]) and their critical role in the metastatic spread of carcinomas was only demonstrated two decades ago; this is because we have only recently possessed technologies with the requisite sensitivity to detect these relatively rare cells in the blood.[6] It was not until the availability of the CellSearch platform (Janssen, Raritan, NJ, USA) in 2004 that the diagnostic value of the epithelial cell adhesion molecule (EpCAM) was verified for CTCs. Specifically, this technology allowed for CTC enumeration across a broad variety of epithelial cancers.[7] The observation that tumor cells overexpress EpCAM has been employed to detect these cells from peripheral blood samples with other approaches as well, including immunocytochemistry,[8] enzyme-linked immunosorbent spot (ELISPOT) assays,[9] and "CellSpotter" systems.[10] For most of these methods, lack of data reproducibility has hindered their widespread adoption, and CellSearch is the only one that has been clinically validated and Food and Drug Administration (FDA)-cleared for enumeration of CTCs in human blood.[11] Today, CTCs have been proposed to serve as biomarkers for the diagnosis and prognostic monitoring of a number of cancers, including (nonexhaustively) metastatic breast, prostate, colorectal, lung, and ovarian cancer.[12] However, their application in the clinical assessment of CCA remains inconclusive since reports related to prognostic significance of CTCs in CCA are scarce, in the data available, CTCs couldn't be detected in all tested samples, limiting their credibility for risk assessment.[13,14]

Quantification of a relatively low number of CTCs against a background of millions of blood cells has thwarted progress in cancer diagnostics, and affinity-based isolation techniques utilizing CTC-specific antigens (e.g., EpCAM, EphB4, HER2, EGFR, MUC-1, CEA, etc.) have not generally addressed this issue.[15,16] Throughput, purity and recovery must all be considered when isolating rare cells from a much larger population of circulating cells, and microfluidic systems featuring small sample volume requirements, multiplexing capabilities and fast processing times, tend to meet such requirements.[17] Moreover, microfluidic approaches can capture live, rare cells such that further cellular, microscopic, or molecular analysis are feasible. This capacity for combining cell isolation and detection methods on a single device opens the door for a plenty of promising possibilities in point-of-care diagnostics.[18] Recently, glycans have been reported to possess major roles in regulating tumor proliferation, metastasis, and angiogenesis, and such molecules have been used alone or in combination with other strategies (e.g., surgery and chemoradiation) for cancer treatment.[19,20] To the best of our knowledge, there are no reported studies on the use of glycosaminoglycans (GAGs) for tumor cell isolation and detection. As antibody-dependent cell sorting has not been completely reliable,[21] we, herein explore the idea of employing the GAG named SCH45[22] for the isolation of CCA CTCs by combining several capture approaches in a shorter period of time, with a significantly lower blood volume on a single device when compared to traditional method. We 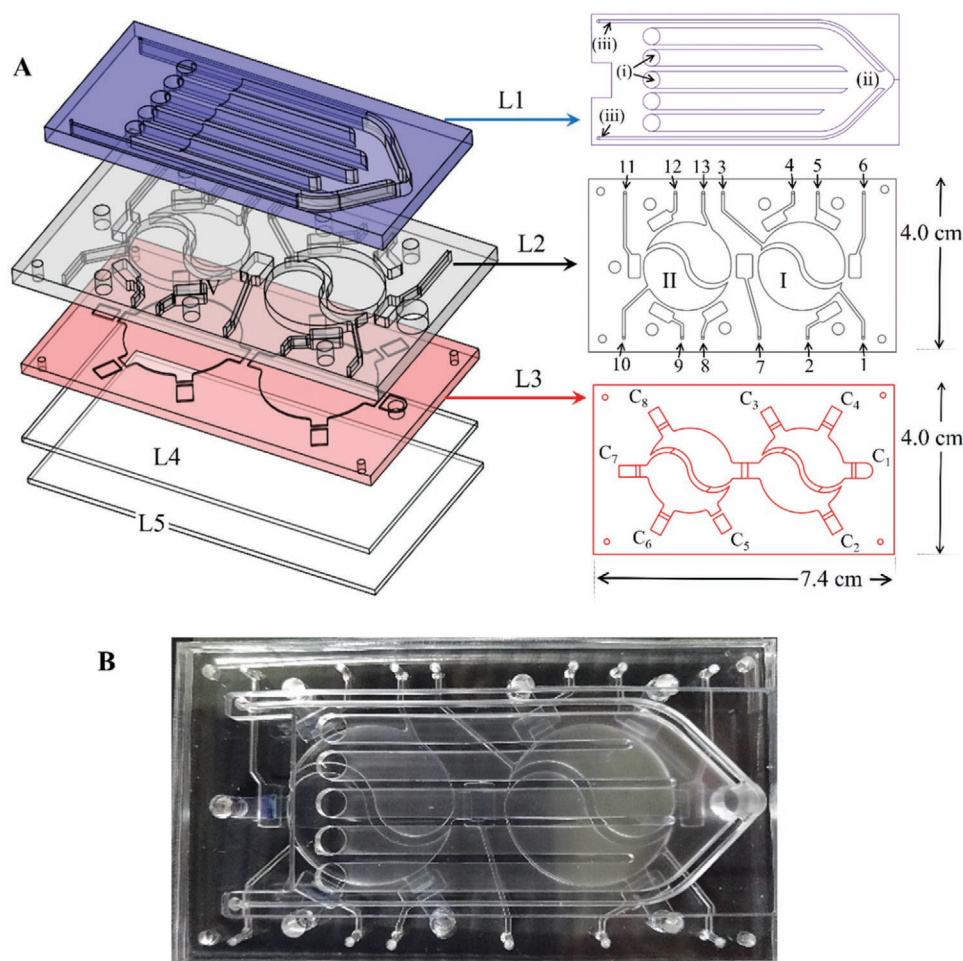report the isolation and detection of CTCs from advanced or metastatic CCA patients' peripheral blood, using a probe, GAG, SCH-45 on an integrated microfluidic platform. The gold standard for CTC enumeration, EpCAM, was used parallelly as a control probe for identifying CTCs from those blood samples. We also attempted to determine whether CTC levels could be predictive of therapeutic efficacies, prior to or alongside radiographic response, in five advanced or metastatic CCA patients.

2. Results

2.1. Microfluidic Device

The pneumatically controlled integrated microfluidic chip was composed of four polydimethysiloxane (PDMS, Sylgard 184A/B, Dow Corning, USA) layers and a double-sided tape layer (3M, USA). The uppermost PDMS layer of the chip was used for collection of cell pellet from blood, and the second and the third layers were the air control and the liquid channel layers, respectively (**Figure 1**A). The fourth (bottom-most) layer of the chip was the thinnest and provided enough support to keep the contents of the liquid channel layer intact. All layers were bonded together via oxygen plasma treatment.[23] The 7.4 cm × 4.0 cm microfluidic chip featured two closed-type micromixer/micropump/transportation units. As shown in Figure 1A, blood after lysis buffer treatment was dispensed into the topmost PDMS layer (L1) through the inlets (i). The channels labelled (iii) served as vent for any bubbles trapped during dispensing lysed blood into the inlets, it also doubled up as waste collection unit for the lysed blood after collection of the pellet. The chamber C_1 was designed such as to ensure no pellet loss after collection and direct transfer of the aforesaid to the micromixer I of the liquid channel layer (L2). The second and third PDMS layers (L2 and L3) of the chip were used for positive enrichment and immunostaining procedures operated pneumatically via active mechanical displacement of two microvalves and an actuation chamber.[24] The air control layer of the chip was divided into two parts; the first micromixer ("I" in Figure 1A) served as the blood treatment unit, in which negative depletion (using magnetic beads surface-coated with anti-CD45 (MB-CD45), for removal of WBCs) and positive enrichment using magnetic beads surface-coated with either SCH45 (MB-SCH45) or the anti-EpCAM Ab (MB-anti-EpCAM) were carried out. The second micromixer ("II" in Figure 1A) served as the immunofluorescence staining chamber. The chip was fabricated and designed such that the collection of pellet, negative depletion, positive (magnetic) enrichment, and immunofluorescence staining could be performed on the same microfluidic platform in a preprogrammed fashion (see "Experimental Section" for details).

In order to isolate CTCs from either healthy or CCA positive patient blood, it was mixed with red blood cell (RBC) lysis buffer and dispensed into the five inlets in the topmost PDMS layer of the chip (L1 in Figure 1A). Each 5.3 cm × 0.5 cm × 0.392 cm microchannel could hold 1038 µL of sample volume amounting to a total volume of ≈5 mL for the entire PDMS layer. A photograph of the integrated microfluidic platform has been shown in Figure 1B. The layers L1 to L5 were bonded together using oxygen plasma treatment

**ADVANCED
SCIENCE NEWS**
www.advancedsciencenews.com
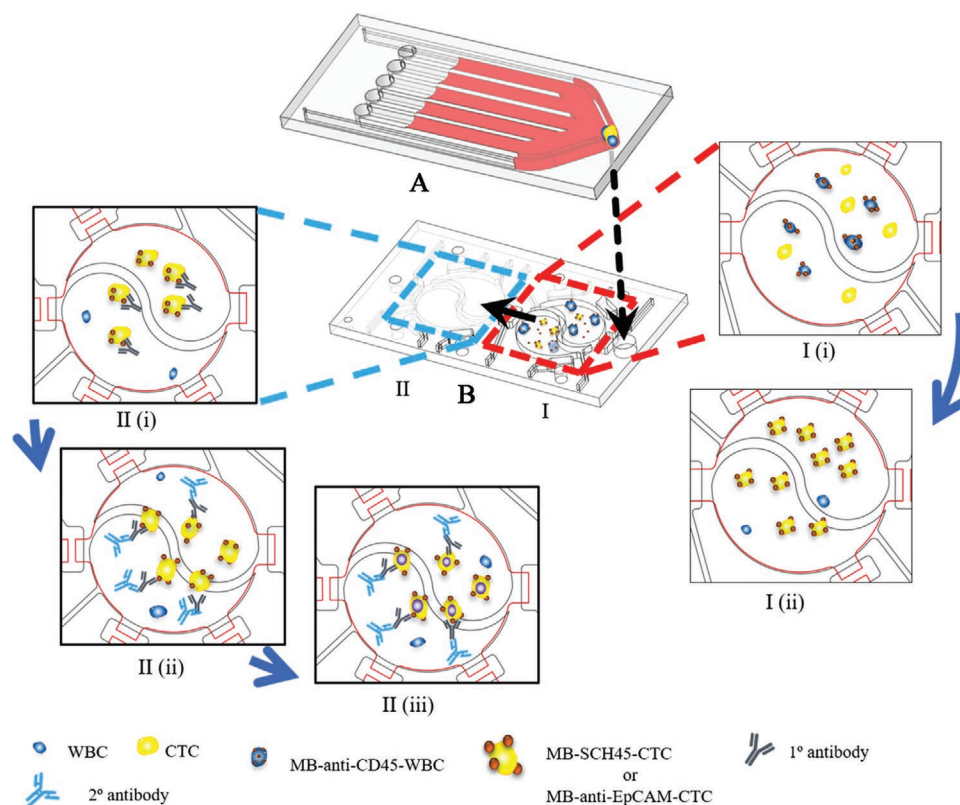
**ADVANCED
HEALTHCARE
MATERIALS**
www.advhealthmat.de

Figure 1. Schematics and photograph of the integrated microfluidic chip. A) A detailed schematic view of the chip featuring all layers from L1 to L5 representing liquid channel layer, air control layer, liquid channel layer, thin PDMS layer, and double-sided tape respectively. Detailed structures of the layers L1, L2, and L3 have been shown where (i) represents inlets for lysed blood, (ii) shows pellet collection area, and (iii) shows outlets for waste collection. (I) represents the blood treatment micromixer and (II) shows the immunofluorescence staining micromixer. The 13 connections to EMVs for pneumatic control of the chip have been represented from 1 to 13. The eight microchambers/reagent storage units have been labeled as C_1 to C_8. C_1: cell pellet collection unit, C_2: waste collection unit, C_3: magnetic bead storage unit, C_4 and C_5: 1X phosphate-buffered saline (PBS) storage unit, C_6: serves as the storage unit for secondary Ab namely DyLight 488 and CD45-PE first and later for DAPI, C_7: waste collection unit, and C_8: anti-CK17 primary (1°) Ab storage unit. B) A photograph of the as fabricated integrated microfluidic chip.

which has been shown to introduce polar functional silanol (SiOH) groups, changing the surface properties of the PDMS microchannels from being hydrophobic to hydrophilic.[25] In addition, treatment with poly(ethylene oxide)-poly(propylene oxide)-poly(ethylene oxide) triblock copolymer (P123) has been shown to induce more hydrophilicity into PDMS surfaces.[26] In this work, both oxygen plasma and P123 treatment were used to ensure that 1) the RBC lysis buffer-treated blood passed through the microchannels with ease and 2) the magnetic beads surface-coated with various Ab or SCH45 did not stick to the walls of the micromixer while performing the negative depletion and positive enrichment steps. Furthermore, the micropumps were capable of transporting the required reagents and samples in a preprogrammed manner such that the whole process could be performed on-chip without major human intervention.

2.2. Characterization of the Micromixers and Micropump

The micromixer used in this study is an active mixer, which also acted as a mechanical displacement micropump. Details on the fabrication of the mixing and pumping units can be found in the experimental section. The relationship between the pumping volume and the gauge pressures was explored to 1) determine the precise amount of fluid dispensed into and from the micromixer/transport unit and 2) to optimize the chip's operating conditions. The maximum pumping volume of the micromixer/micropump unit was determined to be 180 µL at a gauge pressure of −13.33 kPa as shown in Figure S1A (Supporting Information). The maximum pumping volume was likely limited by the release time of the compressed air via PDMS membrane actuation.[27] It is worth noting that the saturation in the pumping volume was achieved at a gauge

**ADVANCED
SCIENCE NEWS**

www.advancedsciencenews.com

**ADVANCED
HEALTHCARE
MATERIALS**

www.advhealthmat.de

Figure 2. Schematics of the on-chip circulating tumor cell (CTC) isolation and detection process. A) PDMS layer containing lysed blood and a pellet containing white blood cells (WBCs) and CTCs acquired upon centrifugation (pellet depicted by yellow and blue color at the apex). B) Air control and liquid control layers of the microfluidic chip with I) blood treatment unit and II) immunofluorescence staining unit. I-i) WBC depletion with MB-anti-CD45. I-ii) Incubation with MB-SCH-45 or MB-anti-EpCAM after collection of the supernatant from the previous step. II-i) mixing of MB-SCH45-cell or MB-anti-EpCAM-cell complexes with primary anti-CK17 Ab. II-ii) mixing with secondary anti-CK17 Ab and CD45-PE. II-iii) mixing with DAPI (nuclear stain).

pressure as low as -19.99 kPa at a frequency of 1 Hz. This could be attributed to the fact that the PDMS membrane had inflated to its maximum capacity, and the air may not have been completely released from the air chamber between cycles; the membrane might also have pressed against the bottom of the chip, allowing no further inflation upon increasing applied air pressure. This is of great significance in this work as the chip was designed such that it could incorporate the 180 µL fluid volume used in negative depletion and positive magnetic enrichment processes by actuation of the pump in less than 2 s.

The mixing efficiency (represented by the mixing index σ) of the micromixer was then investigated (Figure S1B, Supporting Information). In general, the time required for complete mixing decreased with increasing driving frequency. It was also observed that at a driving frequency of 1 Hz, ≈1.2 s was required for complete mixing ($\sigma > 98\%$), while at 5 Hz, the same level of mixing could be achieved in ≈0.6 s. Based upon the above data, the conditions of chip operation were regulated to be a negative gauge pressure of −13.33 kPa and a positive gauge pressure of 6.8 kPa at 2 Hz for negative depletion, positive enrichment and differential immunofluorescence staining since the above processes required gentler mixing conditions such that the magnetic beads surface-coated with affinity reagents had the maximum chances of interaction with the cell surface antigen. Similarly, a negative gauge pressure of −13.33 kPa and a positive gauge pressure of 6.8 kPa at 5 Hz were used for all washing
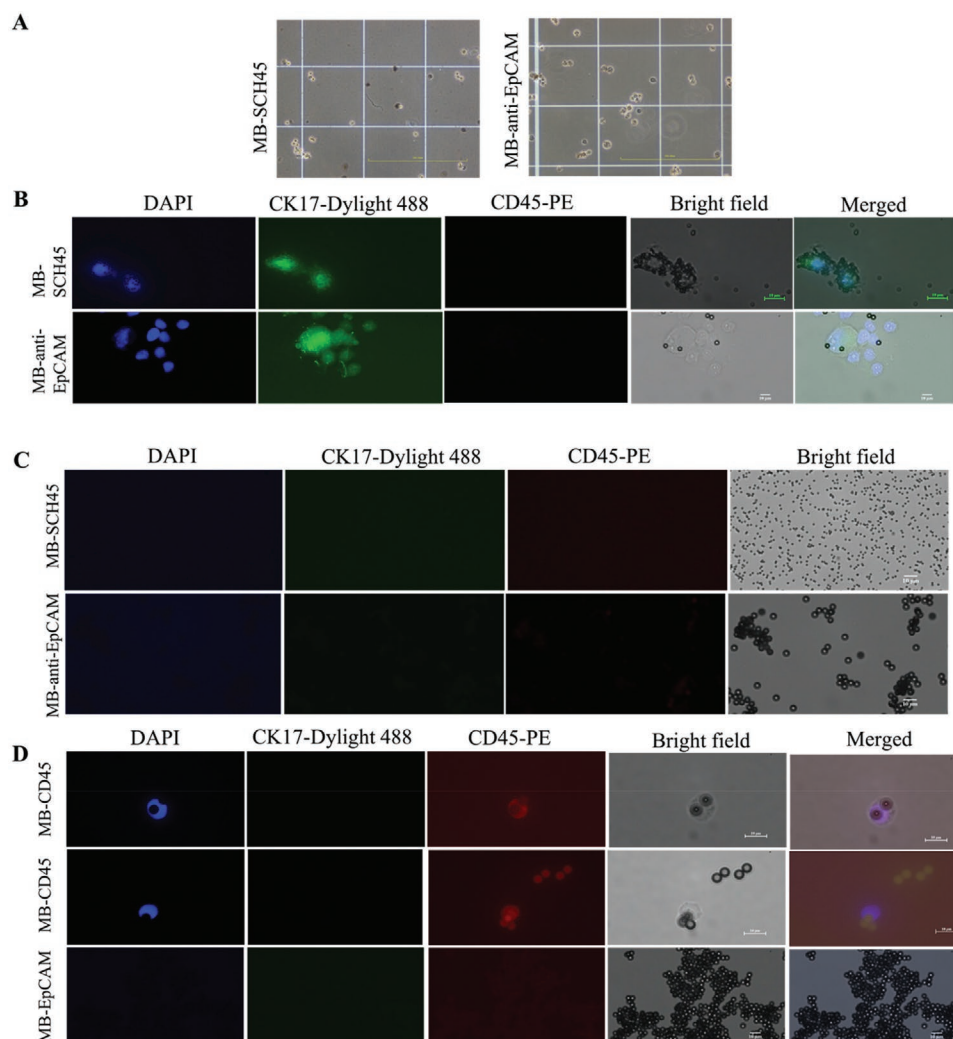
processes to ensure the complete removal of unbound fragments (magnetic beads or Ab) such that the background interference could be greatly reduced.

2.3. CTC Detection on the Integrated Microfluidic Chip

As detailed in the "Experimental section," the experimental process comprised four steps: collection of pellet from the lysed blood, negative depletion of WBCs using MB-anti-CD45, positive enrichment using MB-SCH45 or MB-anti-EpCAM, and immunofluorescence staining. The schematic illustration of the whole process has been detailed in **Figure 2**.

CCA-negative human peripheral blood was first spiked with the intrahepatic CCA cell line, HuH28 to determine whether these cells could be recognized by MB-SCH45 and MB-anti-EpCAM. The rationale for the use of SCH45 with HuH28 has been discussed previously.[22] Briefly, in our previous study, while testing the affinity of ten different glycosaminoglycans toward various cancer cell lines (data not shown here), we observed that SCH45 displayed high affinity and specificity toward the intrahepatic CCA cell line, HuH28. We hypothesized that this probe could be used for CCA CTC isolation from blood. Microscopic observations were made to confirm the efficacy of the method (**Figure 3**). HuH28 cells clearly bound to both MB-SCH45 and MB-anti-EpCAM (Figure 3A),

**ADVANCED
SCIENCE NEWS**

www.advancedsciencenews.com

**ADVANCED
HEALTHCARE
MATERIALS**

www.advhealthmat.de

Figure 3. Results of cell spiking experiments. A) Microscopic observations of HuH28 cells captured by MB-SCH45 and MB-anti-EpCAM. Scale bar: 200 µm. B) Immunofluorescence staining of HuH28 cells captured by MB-SCH45 and MB-anti-EpCAM. C) Immunofluorescence staining of healthy nonspiked blood sample (control) using MB-SCH45 and MB-anti-EpCAM. Only beads are visible. D) Immunofluorescence staining of WBCs captured by MB-anti-CD45. Scale bar: 10 µm. Sample size ($n = 3$).

and average recoveries of 77.8 ± 10.2% and 85.6±12.4% of the spiked cancer cells were observed using MB-SCH45 and MB-anti-EpCAM, respectively. Each experiment was performed in triplicates. Under immunofluorescence microscopy, the isolated HuH28 cells yielded bright fluorescence signals for both anti-CK17-DyLight488 and 4′, 6-diamidino-2-phenylindole (DAPI) but not for CD45-PE (Figure 3B). Three nonspiked blood samples from CCA negative humans served as the control for this experiment (Figure 3C). As observed, neither affinity reagent detected positive cells in the samples from healthy donors nor fluorescence signals were observed. A parallel experiment was also carried out to determine the efficacy of WBC isolation using MB-antiCD45 (Figure 3D), in which no and strong signals were observed for anti-CK17-DyLight 488 and CD45-PE, respectively. After verifying the efficacy and specificity of MB-SCH45 in capturing HuH28 cells spiked into normal blood, we proceeded with blood samples from advanced or metastatic CCA patients.

All 65 advanced or metastatic CCA samples were evaluated using MB-SCH45 and MB-anti-EpCAM on the integrated microfluidic chip, and MB-SCH45 was capable of isolating CTCs from all samples, regardless of the disease status. The number of CTCs isolated from the above samples using MB-SCH45 and MB-anti-EpCAM and details regarding the stage and organ of metastasis have been presented in Table S1 (Supporting Information). It is noteworthy that CTCs could be detected even in the blood of patients (Nos. 5, 14, 23, 30, 32, 43, and 60 in Table S1, Supporting Information) with no distant metastasis as observed by radiographic imaging at the time of observation. We also observed that the size of the CTCs ranged from 5 to 20 µm in diameter (data not shown). Most of the cells presented a high nucleus-to-cytoplasmic ratio but not in all cases. We also documented dramatic heterogeneity in terms of cell shapes among patients as has been documented in other studies.[28]

Experimental data revealed that MB-SCH45 and MB-anti-EpCAM led to the isolation of ≥1 and ≥3 CTCs mL⁻¹ of blood,
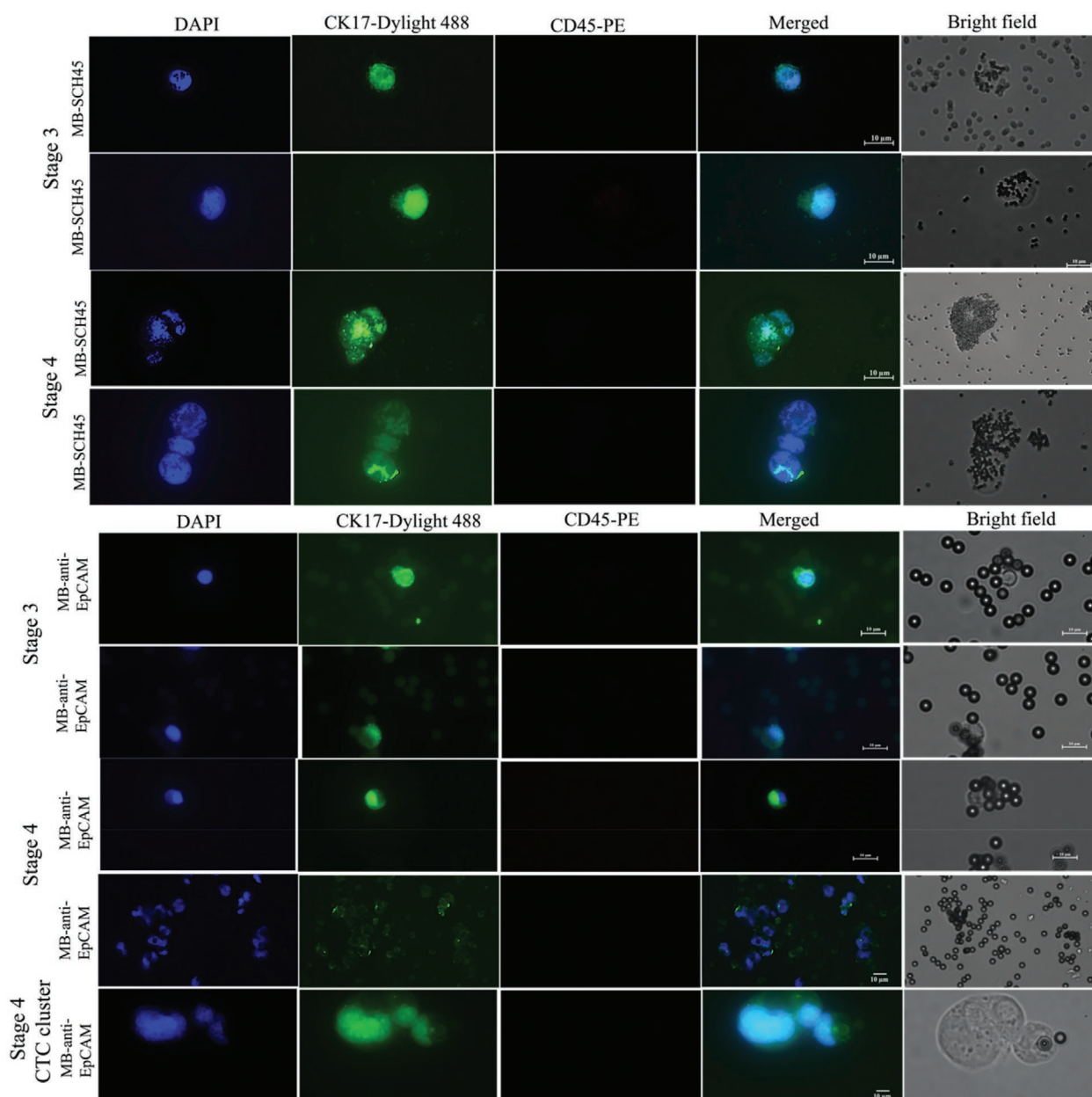
Figure 4. Results of immunofluorescence staining. Negative depletion with anti-CD45 Ab and positive enrichment with MB-SCH45 (top 16 panels) and MB-anti-EpCAM (lower 20 panels) for both representative stage III and stage IV samples. The bottom-most four panels showed the CTC clusters after positive enrichment with MB-anti-EpCAM. Scale bars represent 10×10^{-6} м.

respectively, both of which represent considerable improvements over previous studies.[14,29,30] Furthermore, several stage-IV patients being characterized by the lowest concentrations and nonmetastatic patients displaying significant number of CTCs was also observed.

The immunofluorescence images of some samples have been shown in **Figure 4**. It is worth mentioning that the samples were randomly selected and in no particular order. CTC clusters could be observed using both MB-SCH45 and MB-anti-EpCAM in some stage IV patients. Some clusters were relatively small while others comprised dozens of tumor cells. The CTC clusters were more evident when

MB-anti-EpCAM was used for positive enrichment and have been shown in Figure 4 (the bottom-most 4 panels). Such cluster-forming CTCs are known to have a relatively higher potential for metastasis [31] and should be studied in detail in future works.

2.4. Role of CTCs in Assessing Disease Status

To the best of our knowledge, there have been no reported literature on the effect of chemotherapy on CTC number in CCA patients, till now. This study aimed to demonstrate the correlation
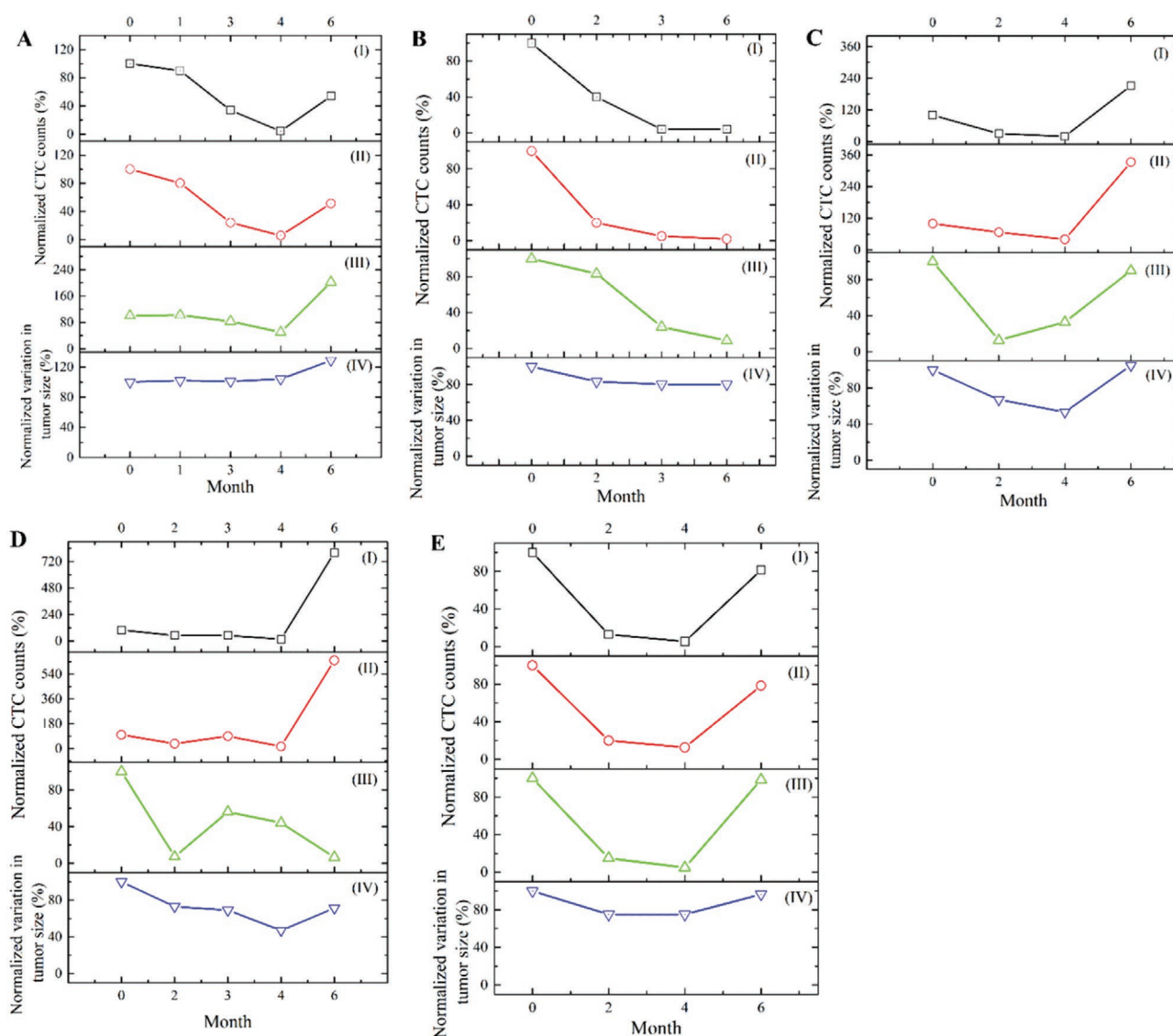
Figure 5. The predictive significance of CTC counts. The correlation between CTC count and clinical response to chemotherapy in five advanced or metastatic CCA patients was tested. Panels A–E represent patients A–E, respectively. Subpanels I–III in each panel represent normalized CTC counts isolated using MB-SCH45, MB-anti-EpCAM, and FACS respectively. Subpanel IV represents the normalized tumor size using radiographic imaging.

(if any) between CTC enumeration and treatment response based on standard radiographic examinations, and to determine whether CTC numbers are symptomatic to treatment response/benefit, prior to or alongside radiographic changes in patients receiving chemotherapy. The number of CTCs and tumor size, before-treatment, were treated as 100% and the after-treatment data pertaining to individual cell number profiles and tumor size measurements were normalized relative to the above, which corresponded to therapeutic outcomes in five advanced or metastatic CCA patients. Detailed information of these five patients with treatment strategy and regimen has been shown in Table S2 (Supporting Information). The results of normalized CTC isolation using MB-SCH45, MB-EpCAM, and flow assisted cell sorting (FACS) alongside computed tomography (CT) scan tumor measurements have been demonstrated in **Figure 5**. CTCs could be successfully detected in all

patients, even after several lines of chemotherapy. The number of CTCs isolated from each sample using MB-SCH45 alongside MB-anti-EpCAM has been detailed in Table S3 (Supporting Information). The total number of CTCs after the first round of treatment decreased when compared with that before treatment in all cases and corresponded with the radiographic response in all cases tested. An increased number of CTCs was observed in patients A, C and D after few lines of chemotherapy which later seemed to corroborate the radiographic finding that the tumor size had increased (implied tumor resistance to chemotherapy) in all these patients. These results not only implied the predictive role of CTC for therapeutic efficacies in all patients but also appeared to prognosticate the response to chemotherapy, often predicting the efficacy of treatment before radiographic results. The data were comparable using MB-SCH45 (patients A, B, and D), or even better (patients C and E) than

Table 1. Literature comparison. Different methods used in the detection of CTCs in cholangiocarcinoma.

Method	Principle	Limitation	Volume of blood used	Reference	Vendor (if available)
Cell Search	Enrichment using ferrofluids with EpCAM antibodies followed by immunostaining for detection	Insufficient sample size	7.5 mL	[37]	Veridex
Cell Search	Enrichment using ferrofluids with EpCAM antibodies followed by immunostaining for detection	Only 22% patients were positive for CTCs	7.5 mL	[17]	Veridex
Cell Search	Enrichment using ferrofluids with EpCAM antibodies followed by immunostaining for detection	Only 23% patients were positive for CTCs	7.5 mL	[15]	Veridex
CytoQuest CR System	Enrichment using ferrofluids with EpCAM antibodies followed by immunostaining for detection on a microfluidic platform	Insufficient sample size	2 mL	[38]	Abnova

FACS analysis. Similar trend was observed in the analysis using MB-EpCAM. Responses were categorized as stable disease, partial response, or disease progression by using response evaluation criteria in solid tumors version 1.1 (RECIST 1.1),[32] as shown in Table S4 (Supporting Information). The finding that changes in CTCs can contemplate tumor's status and response to chemotherapy has already been applied as a reference to assess the efficacy of individualized therapy in metastatic breast and several other cancers.[33] However, to the best of our knowledge, there is limited evidence leading to the above in advanced CCA. Therefore, our preliminary results demonstrate a prognostic and predictive relevance of persisting CTCs during chemotherapy, indicating a potential role of the glycosaminoglycan in therapeutic monitoring of CCA treatment.

3. Discussion

Detection of CTCs has gained immense interest within the cancer research community and this study is the first of its kind to evaluate the feasibility of using the GAG, SCH45 as a probe to isolate CTCs from the peripheral blood of advanced or metastatic CCA patients. This breakthrough is of utmost significance considering the fact that CTCs in CCA have been documented to be extremely rare, with only 17% of patients previously studied displaying positive for CTCs at concentrations ≥ 2/7.5 mL of blood using the FDA-approved CellSearch assay.[14] This is also the first study to isolate CTCs from 100% of the patient samples analyzed (even from patients with no distant metastasis as observed by radiography) using anti-EpCAM as probe. Here, the authors would like to state that this is not a comparison study between the two probes but an attempt at evaluating the new probe. Importantly, the developed microfluidic system involved less human intervention and was characterized by shorter operating times (≈2 h) than its large-scale counterparts (>7.5 h). Previous studies have generally employed the FDA-approved CellSearch system with anti-EpCAM coated magnetic beads which has enabled robust and reliable CTC enumeration in several epithelial tumor types like breast, prostate and colorectal cancers.[28,34,35] However, discrepancies like the detection of very few CTCs in pancreatic cancer patients in comparison with other epithelial carcinomas such as breast, prostate, colorectal and small cell lung cancer have also been reported.[36] With reference to CCA, the CellSearch system was capable of recognizing CTCs in only 23%,[13] 17%,[14] and

62.5%[29] of the patients tested. The capture efficiency seems relatively low with requirement of a considerable amount of blood sample (i.e., 7.5 mL). We used only 1 mL of blood sample for all tests which is about one-seventh of the volume required for the Cell Search assay. This may be attributed to the high capture rates of MB-SCH45 and MB-anti-EpCAM and precise microfluidic chambers. When compared to the number of CTCs isolated using MB-anti-EpCAM, the numbers were relatively smaller for MB-SCH45, as shown in Table S1 (Supporting Information). It might be due to the fact that the levels of expression of the target binding molecule for SCH45 was different on various CTCs leading to the difference between the numbers of CTCs isolated from patient blood in comparison to the spiked sample tests in which MB-SCH45 was capable of isolating ≈79% of the cells while MB-anti-EpCAM isolated ≈86%. Studies also are underway to determine whether the novel GAG could be used for the isolation of EpCAM negative cells.

Furthermore, we analyzed the utility of CTCs as a predictive biomarker in five patients with advanced or metastatic CCA. The sensitivity of tumor to chemotherapy, determined by radiographic imaging is assumed to proximate the clinically meaningful response to therapy in metastatic diseases. However, imaging results are subject to a substantial amount of intra and interobserver bias,[37] and it is not uncommon to find radiographic stability or responsiveness on initial follow-up followed by rapid clinical decline shortly. Our initial results suggest the developed method's superiority over FACS analysis.

Herein we have shown that the developed integrated microfluidic system can successfully detect CTCs from the blood of all advanced or metastatic CCA patients tested and its ability in predicting clinical responsiveness to chemotherapy in five patients. **Table 1** depicts the literature available till date for the isolation and detection of CTCs from CCA patients. As shown in this table, majority of the studies listed have employed Cell Search with questionable significance in the diagnosis or prognosis of CCA as CTCs could be detected in only 22–23% of the patients tested. Another detection platform called CytoQuest CR System from Abnova (Taiwan) has been also developed and tested; however, no clinical data is available for CCA.[38] The developed microfluidic platform was capable of detecting CTCs from 100% samples tested suggesting future prospects of applications in the diagnosis of CCA.

Microfluidic approaches for the isolation of CTCs using affinity techniques have been widely reported[39] offering several advantages of being high throughput, disposable and low

**ADVANCED
SCIENCE NEWS**

www.advancedsciencenews.com

**ADVANCED
HEALTHCARE
MATERIALS**

www.advhealthmat.de

cost of production. The developed microfluidic system provided high recovery of CTCs for advanced or metastatic CCA with shortened process time. The shortened duration may be linked to the effective transport and circulation of the Ab solution around the cell surface antigens in the chip. Our strategy of negative depletion using MB-antiCD45 prior to positive enrichment may also be advantageous as it allows the detection of epithelial cancer cells with the absence of the classical epithelial phenotype potentially permitting a more likely estimation of the number of CTCs.[40]

Since the loss of epithelial markers like EpCAM is a common phenomenon that typically occurs in cancer cells that have undergone the epithelial-mesenchymal transition (a phenomenon which can grant CTCs the ability to enter circulation and seed metastases), it will be critical to identify the exact cellular binding target(s) (ligand) of SCH45 in future works to ensure that all circulating CTCs can be predicted/expected to indeed bind to the MB-SCH45 probes. For that matter, we cannot currently state whether the CTCs captured by MB-SCH45 herein were the same cell types as those captured by MB-anti-EpCAM. Finally, an uncovering of these CCA cell surface ligands may also allow us to develop probes for CTCs specific to only one type of cancer (e.g., CCA), and not CTCs of other cancers. Based upon our experimental results, we articulate that CTCs in CCA may maximize the predictive performance of liquid biopsy for metastatic CCA as well as serve as an effective indicator of treatment efficacy prior to radiographic measurements/changes.

4. Experimental Section

Microfabrication and Design of the Microfluidic Chip: The fabrication process of the pneumatically controlled microfluidic chip has been shown in Figure S2A,G (Supporting Information) which involved 1) micromilling of the poly (methyl methacrylate) (PMMA) mold through a computer-numerical-control (CNC) machining process and 2) molding of the inverse structures in PDMS. The mixing and curing process for PDMS (Sylgard 184A/B, Dow Corning, USA) has been detailed elsewhere.[23] The four layers of the chip were bonded together using oxygen plasma treatment (FC-12064, FEMTO Science, USA) at 90 W for 1 min. The chip was then treated with a solution of Pluronic P123 (MW 5750, 2.5% w/v, Sigma-Aldrich, USA) in 99% (by weight) aqueous ethanol to increase the hydrophilicity of PDMS. P123 was dispensed into the topmost layer of the chip and allowed to react with PDMS for 5 min.

The microvalves were then actuated such that P123 was transported to the blood treatment unit of the chip's liquid layer, then to the micromixer for 15 min, then to the immunofluorescence staining chamber of the chip for 15 min, and finally through the waste collection chamber. The pneumatic microfluidic chip was capable of performing various fluidic functions like mixing, pumping, or transportation using two types of air, compressed air and suction pressure or vacuum. The flow of compressed air or generation of suction pressure was controlled through EMVs. The entire set up for operation of the chip was consisted of an air compressor (S-301, Sharpgun Dental Instrument, Taiwan), a vacuum pump (UN-90 V, Uni-Crown, Taiwan), and a computer controlled EMV functional unit (SMC S070B-SBG-05; Wei-Chia Electro Materials, Taiwan).[41] In a preprogrammed manner, the EMV functional unit automatically switched between the flow of compressed air and generation of vacuum. The operational conditions of the chip as displayed in Table S5 (Supporting Information) were determined after experimental determination of mixing and pumping characteristics (mentioned in the next section) of the chip and therefore unique for every chip.

This chip contained two liquid channel layers and one air control layer; classification is based on the flow of liquid or air across the layer, numerous normally closed microvalves were also integrated into the chip for desirable opening and closing of fluidic channels leading to either flow or no-flow liquid conditions. The microvalves were designed such that a constant flow of compressed air blocks any fluid flow across the channels. When the EMV was switched to a suction pressure or vacuum, the PDMS membranes were deflected, thus opening the channel and leading to fluid flow, as shown in Figure S2G (Supporting Information). The thin PDMS membrane lining the roof of the liquid channel layer, L3 as shown in Figure 1, formed the barrier between the liquid and air layers. Based upon the desired fluidic transport, flow of compressed air or generation of vacuum generates deflection or retraction of the thin PDMS lining leading to fluid flow and various functions on the microfluidic chip. When the micromixer is to be activated, the lining PDMS membrane is actuated at the desired frequency which results in the agitation of liquid in the liquid channel layer leading to uniform mixing as shown in Figure S2H,I (Supporting Information). When it needs to function as a micropump, the pressure generated by the compressed air creates a downward deflection in the lining PDMS membrane; simultaneous opening of the microvalves allows the liquid to be transported out of the chamber. When the pressure is reversed, liquid flows into the chamber. The optimization of these operational parameters of mixing and pumping in this chip has been described later in the text.

Micromixer and Micropump: For the realization of the aforementioned experimental procedures on the microfluidic chip, it was essential to first characterize the components of the microfluidic chip (e.g., micromixers and micropumps) such that the operating conditions could be optimized. The sequential uplifting and deflection of the PDMS membranes in the closed-type micromixer/micropump/transportation unit upon activation by connecting it to an electromagnetic valve (EMV), driven by a custom-made digital controller attached to a vacuum pump (Figure S2H,I, Supporting Information), generated a mixing effect within the chamber. Maximum pumping volume and mixing efficiency were therefore determined as described below.

In order to determine the pumping volume of the micromixer/transport unit, water was used as the medium, and the normally closed microvalves were actuated such that the injected water could be transported from one part of the chamber to another. The tests were conducted at different operating negative gauge pressures ranging from -2.66 to -60 kPa (specifically -2.66, -3.33, -3.99, -4.66, -5.33, -6.66, -13.33, -19.99, -26.66, -33.33, -39.99, -46.66, and -60 kPa) at a pulsation frequency of 1.0 Hz and a positive gauge pressure of -6.8 kPa in triplicates. The transported liquid was collected and weighed to calculate the volume of liquid transported. The rationale behind the use of positive and negative gauge pressure was that the two types of pressures were required for deflection of the PDMS membrane. Positive pressure keeps the membranes deflated under operation while negative pressure inflates them.

The mixing index was commonly used to characterize the effectiveness of the micromixer.[23] In this work, the mixing index of a closed-type micromixer was determined by dispensing 180 μL of deionized (DI) water into the chamber and adding concentrated red ink (2 μL) to it. Pulsation frequencies of 1.0, 2.0, 3.0, 4.0, and 5.0 Hz were applied at an applied gauge pressure of -26.6 kPa, and the mixing process was recorded with a high-speed, charge-coupled device camera (Mikrotron/MC1311, Germany). The images of water and red ink mixing with each other at different time periods were captured at 500 frames s^{-1}, and Image J software (National Institutes of Health, USA) was used to analyze the area to which the ink had spread at different frequencies.

SCH45 Glycosaminoglycan: The GAG used in this study, SCH45, was provided in lyophilized from the Genomics Research Centre (Academia Sinica, Nankang, Taiwan). The structure of this synthetic GAG is composed of four variably sulfated disaccharide units consisting of an N-acetyl-α-D-glucosamine (α-D-GlcNAc), a β-D-glucuronic acid (β-D-GlcA), and an α-L-iduronic acid (α-D-IdoA) linked together by α-1$\rightarrow$4 linkages. The symbols of α-D-GlcNAc, β-D-GlcA, and α-L-IdoA were

respectively defined as ■, ◇, and ◈ such that SCH45 could be represented as ■◇◈■◇■◇◈■◇ (NINGNING).[42] Initially, tetrasaccharide backbones were assembled in a [2 + 2] fashion from the appropriate disaccharide building blocks and convergent [4 + 4] glycosylation provided the fully protected octasaccharide skeleton, which was further subjected to functional group transformations to yield final compound with varying levels of O-sulfonation states. The glycan molecule was then biotinylated such that the resulting compound, SCH45, could be conjugated onto the surface of streptavidin-coated Dynabeads (see the next section for details). Additional structural details of SCH45 could be found in Figure S3 (Supporting Information).

Conjugation of SCH45 to Magnetic Beads: Biotin-labeled SCH45 (100×10^{-6} M concentration) was incubated with Dynabeads MyOne streptavidin C1 (≈ 7–10×10^9 beads mL^{-1}, Ø = 1 µm, Invitrogen, USA) magnetic beads in a volume/volume ratio of 1:10 and placed on an RM-2L INTELLI-mixer (ELMI Ltd., Latvia) at 25 rpm for 30 min at room temperature (C2 mode). The beads were then collected using a magnetic particle concentrator (MPC, Dynabeads MPC-1, Life Technologies) for 2 min. The supernatant was discarded, and the beads were washed thrice with 1 mL of deionized water (DI water). The bead conjugates were suspended in the same volume of DI water as the initial volume of Dynabeads used.

Cell Culture and Spiking Experiments: A human Huh-28 cell line (Resource Identification Initiative (RRID): CVCL_2955, intrahepatic CCA) provided by National Cheng Kung University Hospital (NCKUH) was cultured in Roswell Park Memorial Institute Medium (RPMI 1640, Invitrogen) supplemented with 10% fetal bovine serum (Gibco, USA), 2×10^{-3} M L-glutamine (L-Gln, Gibco), 100 µg mL^{-1} streptomycin (Pen-Strep, Gibco), and 100 U mL^{-1} penicillin-streptomycin (Invitrogen). The cells were incubated in a humidified atmosphere with 5% CO$_2$ at 37 °C. Cells were harvested by incubation with enzyme-free cell dissociation buffer (Thermo-Fisher Scientific, USA) for 10 min at 37 °C. They were then counted using an automated cell counter (TC20, BioRad, US) and their viability was evaluated using trypan blue dye exclusion method. One hundred HuH-28 cells were spiked ($n = 3$ replicate cell aliquots) into 1 mL of blood from three healthy donors, and negative depletion of WBCs followed by positive enrichment with MB-SCH45 and MB-anti-EpCAM were carried out as described below. Cell-bead complexes were isolated using a magnet and then washed with wash buffer. The cells were counted using a hemocytometer (Neubauer-improved counting chamber, Marienfeld, Germany), and the percentage of cells isolated using MB-SCH45 and MB-anti-EpCAM were divided by the total number of initially loaded cells to calculate the isolation efficiency. The cells were also subjected to immunofluorescence staining as described below to verify potential contamination with WBCs.

Blood Specimen Collection: This study was approved by the ethics review committees of NCKUH (IRB No. A-ER-103-063), and informed written consent was obtained from all 65 advanced stage or metastatic CCA patients. The three healthy blood samples used in this study were collected from Tainan blood bank, Taiwan. For each donor, peripheral blood (10 mL) was drawn into BD Vacutainer spray coated K2EDTA tubes (BD Diagnostics, USA). All samples were maintained and transported at 4 °C and processed within 30 h of collection. To avoid bias, samples were blindly processed without prior information on the disease status, cancer stage, or metastasis in patients.

Experimental Set-Up: The experimental procedure involved four steps: 1) RBC lysis and isolation of pellet, 2) negative depletion for the removal of WBCs, 3) positive magnetic enrichment, and 4) immunofluorescence staining. Table S6 (Supporting Information) lists chip operation conditions, volume of reagents and gauge pressures used, and each step is described in more detail below.

Experimental Set-Up—RBC Lysis and Pellet Collection: RBC were lysed by adding 9 mL of 1X RBC lysis buffer (Biolegend, USA) to 1 mL of peripheral blood and incubating at room temperature with gentle mixing on a rotary shaker (TKS ROCKER-RS-01, Lab666, Taiwan) for

5 min. Then the sample was dispensed into the topmost PDMS layer of the chip through the inlets provided (Figure 1A). The microfluidic chip was then spun as described above and placed on a PMMA plate with a groove such that the microfluidic chip could be placed inside it. It was then placed on a spin-coater (M and R Nanotechnology Co. Taoyuan, Taiwan) and spun at 1200 rpm for 2 min at a negative gauge pressure of -67 kPa and the cell pellet was then moved into the blood treatment unit of the chip's liquid channel layer by a vacuum force created by the microvalves. The waste blood with lysed RBCs was removed through the waste outlets (marked as (iii) in Figure 1A) using vacuum suction. The remaining 5 mL of lysed blood was then dispensed into the topmost layer of the microfluidic chip and the above process was repeated. The pellet was transported to the micromixer and suspended in 180 µL of 1X phosphate buffered saline (PBS) by activating the micromixer for 2 min. The resulting cell suspension consisting of predominately nucleated cells was then subjected to negative depletion for the removal of leucocytes as described below and in a prior study.[43]

Experimental Set-Up—Negative Depletion and Positive Magnetic Enrichment: A negative depletion strategy reliant on the removal of leucocytes via their binding to anti-CD45 Ab bound to magnetic beads (Dynabeads CD45, Thermo-Fisher Scientific) was employed herein on-chip. The cell-bead complexes were then attracted to a magnet to remove the bound leukocytes from the lysed blood samples. After four rounds of negative depletion, the remaining cells (predominantly CTCs) in the collected supernatant were mixed with MB-SCH45 (described above) or MB-anti-EpCAM (EpiEnrich, 4×10^8 beads mL^{-1}, Ø = 4.5 µm, Thermo-Fisher Scientific). The magnetic bead-CTC complexes were then collected, washed, and transferred to the immunofluorescence staining unit of the chip for further analysis (described below).

Experimental Set-Up—Immunofluorescence Staining: For immunofluorescence staining, primary anti-CK17 (1:500 dilution; 100 µL, 0.6 mg mL^{-1}, GTX103765, Rabbit, GeneTex, USA) was used. The secondary Ab, goat antirabbit IgG DyLight 488; GeneTex and anti-CD45-PE (RRID: AB_10375163, HU CD45 PE, Life Technologies) were used at a dilution of 1:500. It is to be noted here that the anti-CD45 Ab used had a PE tag thereby requiring no primary Ab. DAPI (1 mg mL^{-1}, Thermo Fischer, US) was then used as the nuclear stain. After the final magnetic collection, the bead-cell complexes were suspended in 10 µL of 1X PBS and collected through the waste collection chamber. They were transferred onto the numbered microscopic slide and ProLong Gold Antifade Reagent (Invitrogen) was used to embed the cell-bead complexes.

The numbered microscope slide was fabricated using an SU-8 standard photolithography process[44] to facilitate CTC counting. Concisely, a 30 µm thick layer of SU-8 3035 (MicroChem, USA) was spin-coated on a glass microscope slide. A soft-baking process for 10 min was performed and the SU-8 microstructures were patterned at a dosage of 147 mJ cm^{-2} of ultraviolet light exposure. A postexposure bake at 65 °C for 1 min and 95 °C for 5 min was performed followed by a standard SU-8 developing process. The glass slide featuring the microstructures was formed and the as fabricated numbered microscope slide using biocompatible SU-8 patterning has been documented in Figure S4A–D (Supporting Information). The Huh28 cells captured using MB-SCH45 in the cell spike experiments has also been shown in Figure S4E (Supporting Information). The slides were then analyzed under the microscope using a DS-Qi1Mc camera equipped with a Peltier cooling device and a programmable gain amplifier (Nikon) coupled to an inverted microscope equipped with a digital control module. The software used was NIS-Elements Basic Research software (Br, version 4.20.00, 64 bit, Nikon). A cell was considered to be CTC if it 1) expressed CK (an internal architectural protein that is largely associated with epithelial cells), 2) was characterized by a high nuclear: cytoplasmic ratio (upon DAPI staining), and 3) did not express CD45.

Assessment of CTCs in Metastatic CCA Patients before and after Chemotherapy: The role of CTCs was investigated in response to treatment effectiveness assessment by analyzing blood samples (1 mL) before and after chemotherapy in five patients with advanced or

1901875 (10 of 12)

metastatic CCA for a period of six months. The presence and number of CTCs in blood were assessed using the prior mentioned MB-SCH45 alongside MB-anti-EpCAM followed by immunofluorescence staining along with the conventional FACS and tumor size measurements were performed using CT scan. For CT scan measurements, the solid tumors were measured in at least one dimension with the longest diameter as per RECIST guidelines, CT scan of a patient has been displayed in Figure S5 (Supporting Information). Before initiating chemotherapy, baseline studies of CTC enumeration from blood and radiographic analysis were performed within an average of 3 d prior to starting treatment. Blood samples from five CCA patients were obtained at 4–12-week intervals and the same type of imaging studies were performed with an average of 4 d between imaging and the blood draw.

Statistical Analysis: The sample size (*n*) has been presented in the pertinent figure legends. Details regarding data normalization (for before and after chemotherapy patients) have been described in the Experimental Section. Statistical analysis was performed using OriginPro (OriginLab, Massachusetts, USA).

Supporting Information

Supporting Information is available from the Wiley Online Library or from the author.

Conflict of Interest

The authors declare no conflict of interest.

[1] B. Blechacz, *Gut Liver* **2017**, *11*, 13.
[2] T. Ikenoue, Y. Terakado, H. Nakagawa, Y. Hikiba, T. Fujii, D. Matsubara, R. Noguchi, C. Zhu, K. Yamamoto, Y. Kudo, Y. Asaoka, K. Yamaguchi, H. Ijichi, K. Tateishi, N. Fukushima, S. Maeda, K. Koike, Y. Furukawa, *Sci. Rep.* **2016**, *6*, 23899.
[3] B. Blechacz, B. Komuta, T. Roskams, G. J. Gores, *Nat. Rev. Gastroenterol. Hepatol.* **2011**, *8*, 512.
[4] M. O. Wang, C. E. Vorwald, M. L. Dreher, E. J. Mott, A. Cinar, H. Mehdizadeh, S. Somo, D. Dean, E. M. Brey, J. P. Fisher, *Adv. Mater.* **2016**, *27*, 138.
[5] T. R. Ashworth, *Aust. Med. J.* **1869**, *14*, 146.
[6] C. M. M. Court, J. S. S. Ankeny, S. Sho, J. S. S. Tomlinson, *Cancer Treat. Res.* **2016**, *168*, 345.
[7] L. Wang, P. Balasubramanian, A. P. Chen, S. Kummar, Y. A. Evrard, R. J. Kinders, *Semin. Oncol.* **2016**, *43*, 464.
[8] A. Wirtschafter, M. S. Benninger, T. J. Moss, T. Umiel, K. Blazoff, M. J. Worsham, *Arch. Otolaryngol., Head Neck Surg.* **2002**, *128*, 40.
[9] A. Kuske, T. M. Gorges, P. Tennstedt, A.-K. Tiebel, R. Pompe, F. Preißer, S. Prues, M. Mazel, A. Markou, E. Lianidou, S. Peine, C. Alix-Panabières, S. Riethdorf, B. Beyer, T. Schlomm, K. Pantel, *Sci. Rep.* **2016**, *6*, 39736.
[10] A. Toss, Z. Mu, S. Fernandez, M. Cristofanilli, *Ann. Transl. Med.* **2014**, *2*, 108.
[11] S. de Wit, G. van Dalum, L. W. M. M. Terstappen, *Scientifica* **2014**, *2014*, 819362.
[12] W. J. Allard, J. Matera, M. C. Miller, M. Repollet, M. C. Connelly, C. Rao, A. G. J. Tibbe, J. W. Uhr, L. W. M. M. Terstappen, *Clin. Cancer Res.* **2004**, *10*, 6897.
[13] O. Al Ustwani, D. Iancu, R. Yacoub, R. Iyer, O. Al Ustwani, D. Iancu, R. Yacoub, R. Iyer, *J. Gastrointest. Oncol.* **2012**, *3*, 97.
[14] J. D. Yang, M. B. Campion, M. C. Liu, R. Chaiteerakij, N. H. Giama, H. Ahmed Mohammed, X. Zhang, C. Hu, V. L. Campion, J. Jen, S. K. Venkatesh, K. C. Halling, B. R. Kipp, L. R. Roberts, *Hepatology* **2016**, *63*, 148.
[15] N. Gerges, J. Rak, N. Jabado, *Br. Med. Bull.* **2010**, *94*, 49.
[16] T. Ohnaga, Y. Shimada, K. Takata, T. Obata, T. Okumura, T. Nagata, H. Kishi, A. Muraguchi, K. Tsukada, *Mol. Clin. Oncol.* **2016**, *4*, 599.
[17] L. Hajba, A. Guttman, *TrAC, Trends Anal. Chem.* **2014**, *59*, 9.
[18] Y. Dong, A. M. Skelley, K. D. Merdek, K. M. Sprott, C. Jiang, W. E. Pierceall, J. Lin, M. Stocum, W. P. Carney, D. A. Smirnov, *J. Mol. Diagn.* **2013**, *15*, 149.
[19] Basappa, K. S. R, K. Sugahara, *Glycoconjugate J.* **2014**, *31*, 461.
[20] M. Belting, *Thromb. Res.* **2014**, *133*, S95.
[21] P. Potdar, N. Lotey, *J. Cancer Metastasis Treat.* **2015**, *1*, 44.
[22] W. C. Tsai, L. Y. Hung, T. Y. Huang, Y. S. Shan, S. C. Hung, G. B. Lee, in *2017 IEEE 12th Int. Conf. Nano/Micro Eng. Mol. Syst. NEMS 2017*, IEEE, Los Angles, CA **2017**, pp. 489–493.
[23] A. Sinha, P. Gopinathan, Y. Da Chung, H. Y. Lin, K. H. Li, H. P. Ma, P. C. Huang, S. C. Shiesh, G. B. Lee, *Biosens. Bioelectron.* **2018**, *122*, 104.
[24] C. H. Weng, K. Y. Lien, S. Y. Yang, G. B. Lee, *Microfluid. Nanofluid.* **2011**, *10*, 301.
[25] H. Hillborg, J. F. Ankner, U. W. Gedde, G. D. Smith, H. K. Yasuda, K. Wikström, *Polymer.* **2000**, *41*, 6851.
[26] C. J. Huang, H. I. Lin, S. C. Shiesh, G. Bin Lee, *Biosens. Bioelectron.* **2012**, *35*, 50.
[27] C. J. Huang, H. I. Lin, S. C. Shiesh, G. B. Lee, *Biosens. Bioelectron.* **2012**, *35*, 50.
[28] J. S. de Bono, H. I. Scher, R. B. Montgomery, C. Parker, M. C. Miller, H. Tissing, G. V. Doyle, L. W. W. M. Terstappen, K. J. Pienta, D. Raghavan, *Clin. Cancer Res.* **2008**, *14*, 6302.
[29] J. D. Yang, M. B. Campion, R. Chaiteerakij, T. A. Mettler, N. H. Giama, V. L. Campion, K. C. Halling, L. R. Roberts, *Gastroenterology* **2011**, *140*, S921.
[30] R. Giovannoni, A. Villanueva, *Hepatology* **2016**, *63*, 23.
[31] A. Fabisiewicz, E. Grzybowska, *Med. Oncol.* **2017**, *34*, 12.
[32] E. A. Eisenhauer, P. Therasse, J. Bogaerts, L. H. Schwartz, D. Sargent, R. Ford, J. Dancey, S. Arbuck, S. Gwyther, M. Mooney, L. Rubinstein, L. Shankar, L. Dodd, R. Kaplan, D. Lacombe, J. Verweij, *Eur. J. Cancer* **2009**, *45*, 228.
[33] K. Ried, P. Eng, A. Sali, *Adv. Cancer Prev.* **2017**, *02*, 2275.
[34] S. J. Cohen, C. J. A. Punt, N. Iannotti, B. H. Saidman, K. D. Sabbath, N. Y. Gabrail, J. Picus, M. Morse, E. Mitchell, M. C. Miller, G. V. Doyle, H. Tissing, L. W. M. M. Terstappen, N. J. Meropol, *J. Clin. Oncol.* **2008**, *26*, 3213.
[35] M. Cristofanilli, G. T. Budd, M. J. Ellis, A. Stopeck, J. Matera, M. C. Miller, J. M. Reuben, G. V Doyle, W. J. Allard,

**ADVANCED
SCIENCE NEWS**

www.advancedsciencenews.com

**ADVANCED
HEALTHCARE
MATERIALS**

www.advhealthmat.de

L. W. M. M. M. M. Terstappen, D. F. Hayes, *N. Engl. J. Med.* **2004**, *351*, 781.

[36] L. Khoja, A. Backen, R. Sloane, L. Menasce, D. Ryder, M. Krebs, R. Board, G. Clack, A. Hughes, F. Blackhall, J. W. Valle, C. Dive, *Br. J. Cancer* **2012**, *106*, 508.

[37] P. Thiesse, L. Ollivier, D. Di Stefano-Louineau, S. Négrier, J. Savary, K. Pignard, C. Lasset, B. Escudier, *J. Clin. Oncol.* **1997**, *15*, 3507.

[38] S. Wang, K. Liu, J. Liu, Z. T. F. Yu, X. Xu, L. Zhao, T. Lee, E. K. Lee, J. Reiss, Y. K. Lee, L. W. K. Chung, J. Huang, M. Rettig, D. Seligson, K. N. Duraiswamy, C. K. F. Shen, H. R. Tseng, *Angew. Chemie - Int. Ed.* **2011**, *50*, 3084.

[39] S. Wang, K. Liu, J. Liu, Z. T. F. Yu, X. Xu, L. Zhao, T. Lee, E. K. Lee, J. Reiss, Y. K. Lee, L. W. K. Chung, J. Huang, M. Rettig, D. Seligson,

K. N. Duraiswamy, C. K. F. Shen, H. R. Tseng, *Angew. Chem., Int. Ed.* **2011**, *50*, 3084.

[40] Z. Liu, A. Fusi, E. Klopocki, A. Schmittel, I. Tinhofer, A. Nonnenmacher, U. Keilholz, *J. Transl. Med.* **2011**, *9*, 70.

[41] P. Gopinathan, A. Sinha, Y. Da Chung, S. C. Shiesh, G. B. Lee, *Analyst 144*, 4943, **2019**.

[42] Y. P. Hu, S. Y. Lin, C. Y. Huang, M. M. L. Zulueta, J. Y. Liu, W. Chang, S. C. Hung, *Nat. Chem.* **2011**, *3*, 557.

[43] L. Yang, J. C. Lang, P. Balasubramanian, K. R. Jatana, D. Schuller, A. Agrawal, M. Zborowski, J. J. Chalmers, *Biotechnol. Bioeng.* **2009**, *102*, 521.

[44] Y. H. Chen, A. K. Pulikkathodi, Y. D. Ma, Y. L. Wang, G. B. Lee, *Lab Chip 19*, 618, **2019**.

1901875 (12 of 12)